Steady-State Electrorheology of Nematic Poly(*n*-hexyl isocyanate) Solutions

Kwok-Leung Tse[†] and Annette D. Shine*

Department of Chemical Engineering, University of Delaware, Newark, Delaware 19716

Received September 17, 1999; Revised Manuscript Received February 10, 2000

ABSTRACT: The steady-state electrorheological (ER) properties of unidomain nematic poly(*n*-hexyl isocyanate) (PHIC) solutions in *p*-xylene have been experimentally characterized and theoretically modeled with a two-dimensional modified version of Doi's theory of liquid crystalline polymer rheology. This molecular model allows the prediction of ER fluid behavior directly from properties of the component polymer and solvent. Optical conoscopic measurements confirmed that high applied electric fields align the PHIC molecules in the field direction, so the high-field viscosity approaches the transverse Miesowicz viscosity, η_c. The PHIC solutions exhibited many desired ER properties comparable to strong suspension ER fluids, such as a transmitted shear stress of 16 kPa and a viscosity enhancement of 180 times. At low shear rates, quantitative agreement between predictions and data at high fields was obtained using a single adjustable parameter, the rotational diffusivity, D_r. At high shear rates, an additional parameter, β, was required to account for the viscous contributions to the stress tensor. The temperature dependence of the solution electrorheology was predicted to come exclusively from that of the solvent viscosity.

Introduction

Electrorheological (ER) fluids undergo a large, rapid alteration of rheological properties when subjected to an external electric field. First discovered by Winslow[1] in 1949, most ER fluids consist of a suspension of small, polarizable particles dispersed in a nonpolar liquid. Application of an electric field induces the formation of chains of particles along the field direction; these chains are responsible for the increased resistance to flow perpendicular to the chains. Several recent reviews summarize the properties and applications of suspension ER fluids.[2−4]

Unfortunately, suspension ER fluids possess several major disadvantages which have so far kept them from commercialization. The suspensions exhibit particle attrition and settling, especially over prolonged times. Perhaps more significantly, it is still not possible to predict ER suspension properties directly from component properties, composition, and operating conditions,[2] despite 50 years of research. This lack severely impedes the development of new fluid formulations with improved properties.

In an effort to overcome disadvantages of suspension ER fluids, researchers in the past decade have begun to examine homogeneous (nonparticulate) ER fluids based on liquid crystals, especially liquid crystalline polymers (LCPs). The ER effect has been explored in main-chain LCPs with flexible spacers between mesogens,[5] in side-chain LCPs with a flexible backbone having attached mesogens,[5−7] and in solutions of rigid rod main-chain LCPs,[8,9] especially those having a helical structure.[10−13]

The ER effect observed in LCPs arises from the anisotropy of the mesogen shape and of the attendant electrical properties. Application of an electric field to an elongated mesogen of positive dielectric anisotropy acts on the rigid segment to orient it parallel to the electric field direction. If the field is applied perpendicular to the flow direction, then the viscosity of the fluid is considerably larger than the viscosity without electric field. Of course, this orientation may be partially frustrated by spacer groups or supramolecular structure. With low-frequency or dc fields, electrohydrodynamic instabilities may also occur.[14]

The electrorheological effect in LCPs can be substantial; maximum transmitted stress values ranging from 1.7 to 3.0 kPa have been reported.[5,6,10] Most LCP ER fluids are single-phase solutions which are amenable to treatment by continuum theories, so prospects for modeling their ER behavior may be brighter than for suspensions. Yang and Shine[10] successfully described the steady-state electroviscosity of their poly(*n*-hexyl isocyanate) (PHIC) solution at a shear rate of 0.4 s^{-1} using a two-dimensional version of the Ericksen−Leslie−Parodi (ELP) theory.[15] However, ELP theory is a linear, phenomenological theory which has four empirical parameters, so its predictive usefulness is limited to slow flows and to fluids which are well-characterized experimentally. Jamieson and co-workers[8] have used the theory of Brochard[16] to describe the ER viscosity enhancement of dilute solutions of main-chain LCPs dissolved in low molecular weight liquid crystals. The ratio of increments in the Miesowicz viscosities η_c and η_b of the solvent is determined from the root-mean-square end-to-end distance of the polymer chain measured perpendicular and parallel to the director. However, the theory has not yet been adapted for predicting ER properties since it does not incorporate electric field strength as a variable.

A more promising theory for describing the ER behavior of LCPs is the molecular theory of Doi[17] for rigid-rod polymer rheology. By inclusion of a dipolar potential, Tse and Shine[18] have modified the two-dimensional version of Doi theory developed by Marrucci and Maffetone[19,20] to permit predictions of steady-state and transient viscosity, as well as of the linear viscoelastic properties. The model successfully described the data of Yang and Shine[10] for PHIC, as well as the

* Corresponding author.
[†] Current address: VM Technology, Infineum USA L. P., 1900 East Linden Avenue, Linden, NJ 07036.

10.1021/ma991585o CCC: $19.00
Published on Web 03/23/2000

limited data of Tse and Shine[11] for solutions of poly(*n*-hexyl-L-glutamate) in *p*-xylene. Because this model is a molecular theory, it is based on molecular parameters such as the dipole moment, μ, and the rotary diffusion coefficient, D_r, of the LCP.

In this paper, we present experimental ER characterization of PHIC solutions undergoing steady-state shear flow. Specifically, we examine the effects of temperature, concentration, shear rate, and electric field strength on the electroviscosity and normal stress of solutions of PHIC in *p*-xylene. Polymer molecular weight was not varied in these experiments. The experimental data collected are then used to test our previously developed model[18] under a wide range of conditions.

Experimental Section

Poly(*n*-hexyl isocyanate) was synthesized by anionic polymerization following the procedure by Shashoua et al.[21] The polymer had a polydispersity, $\overline{M_w}/\overline{M_n}$, of 2.9 as characterized by gel permeation chromatography and a viscosity average molecular weight, $\overline{M_v}$, of 100 000 obtained by intrinsic viscosity measurements. In toluene solution at 25 C, this molecular weight would correspond to 3.65 persistence lengths.[22] When observed under crossed polarizers, the solution was birefringent in *p*-xylene when the concentration was ≥22 wt % and appeared completely nematic when the concentration was ≥26 wt %. The critical concentration, *c**, above which the isotropic phase becomes unstable is estimated to be 26.3 wt % on the basis of Onsager theory.[23] Solutions with concentrations of 26, 28, and 30 wt % were used in the rheological characterization. Because *c*/*c** of the solutions used in the experiments was near unity and because the zero-field steady-state viscosity did not show region I behavior, we do not expect that defects or textures in the LCP solutions are influential in the electrorheology.

The permanent dipole moment of PHIC of various molecular weights in toluene has been reported by Block et al.[24] For a PHIC with $\overline{M_v}$ of 115 000, Block determined the effective permanent dipole moment at high fields to be 4.7×10^{-27} C m in toluene. Assuming a spherical cavity and using a cavity field factor of 1.5 yields a value of 3.8×10^{-27} C m for the intrinsic permanent dipole moment of our 100 000 $\overline{M_v}$ PHIC.

All ER characterization was performed on a Rheometrics RMS 800 rotational rheometer using a parallel plate geometry. The rheometer was modified by Rheometrics to perform ER characterization (electrorheological material analysis option), which allows simultaneous application of computer-controlled shear rate and electric field during the measurements. The steady-state electroviscosity and the normal stress, $N_1 - N_2$, were measured according to the procedure developed by Yang and Shine.[10] Shear rates and dc electric field strengths up to 100 s^{-1} and 4 MV/m were used, respectively. Because of the use of parallel plates, the shear rate reported here is the edge shear rate. A cup and plate fixture equipped with solvent-soaked humidity pads was used to retard solvent evaporation; this was essential for experiments conducted at elevated temperatures. A disposable fixture with a stainless steel plate of diameter 35 or 25 mm was used as the upper plate. Gap size was varied from 0.4 to 0.9 mm. In particular, high shear rate data were obtained with the 25 mm plate and a 0.4 mm gap size to prevent sample edge fracture. Rheological data were measured at room temperature (typically 23 °C), unless otherwise specified. Experiments were also conducted at 13, 37, and 52 °C with the optional fluids bath designed for the RMS 800 rheometer. Since the effect of moisture on the ER properties of LCP solutions is unknown, the fluids bath with water as the circulating medium was modified to eliminate direct exposure of the polymer solution to moisture. Reproducibility experiments were performed and included solutions made and tested on different days, using different plate fixtures and gap sizes. The standard deviation of zero-field viscosity measurements was 6.4%, for shear rates ranging from 0.3 to 100 s^{-1}. For electroviscosity measurements, the standard deviation was comparable to that for the zero-field case, provided the applied field was either relatively low (<0.15 MV/m) or relatively high (>1.0 MV/m). At intermediate fields, where the viscosity undergoes a rapid increase with increasing electric field, the standard deviation of repeat measurements was as high as 27%; this deviation is presumably due to uncertainties in the value of the applied field.

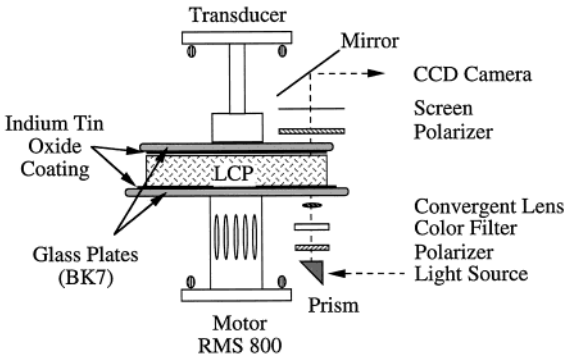

Figure 1. Electrorheooptical apparatus.

To confirm that the ER effect in the PHIC solutions results from director orientation, a glass flow cell was designed and fabricated for the RMS 800 to perform electrorheological and optical measurements simultaneously. The upper glass plate (BK7 optical quality glass), 50 mm in diameter and 3 mm in thickness, was mounted on a custom-made stainless steel fixture to provide enough clearance for the optical components, while the lower glass plate, 65 mm in diameter and 3 mm in thickness, was mounted on a Rheometrics disposable fixture. The surfaces of the glass plates making contact with the solution were vacuum-coated with a transparent indium tin oxide (ITO) coating about 200 nm thick to serve as an electrode. The electrical resistivity of ITO is approximately the same as that of tin oxide, which is 300 Ω/cm^2.[25] The resistance of the ITO coating was estimated to be 1.2×10^{-7} Ω, which is about 10^4 times that of steel with the same dimensions. This relatively high resistance coating could cause the effective electric field in the sample to be less than that applied across lower resistance electrodes such as stainless steel.

The optical train consisted of a typical conoscopy setup.[26] A red or a blue color filter was necessary to eliminate birefringence arising from white light in the interference patterns. The conoscopic interference patterns were captured by a CCD camera, saved on tape, and analyzed using the image processing software Image 1.59b1 by the National Institutes of Health. The electrorheooptical (ERO) setup is schematically depicted in Figure 1. Further details of the setup can be found elsewhere.[27] In this way, the electroviscosity data could be correlated with the conoscopic observations, and the director orientation and the unidomain structure could be verified. Sample thicknesses of 0.6 and 0.9 mm were used with the ERO cell. The size of the upper glass plate prevented using electric field strengths higher than 2 MV/m, due to overload of the normal force transducer.

The ITO coating did not produce any undesirable effect in the absence of an electric field, since the zero-field steady state viscosity data obtained with the glass and the stainless steel plates were in excellent agreement. However, the attractive normal stress of a quiescent PHIC solution measured with the glass plates was consistently smaller (by as much as 20%) than that with the stainless steel plates at the same applied field. This was presumed to be the result of a reduced electric field in the gap due to the electrical resistance of the ITO coating. Hence, a value of the electric field corrected for the coating resistance was taken to be the electric field needed to be applied across stainless steel plates in order to produce the same quiescent normal stress seen in the ERO at a given value of the applied electric field. Results of the steady-state electroviscosity obtained with the glass plates and with the electric field corrected by this procedure were in good agreement with

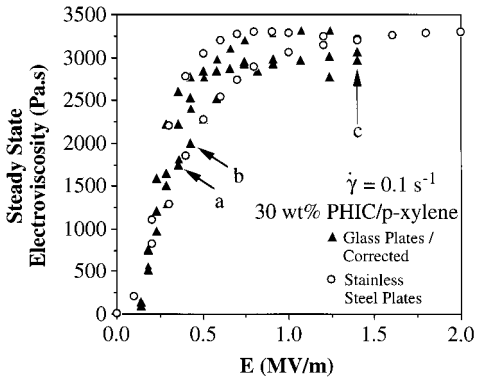

Figure 2. Steady-state electroviscosity of 30 wt % PHIC solution at a shear rate of 0.1 s^{-1}. Open circles are measurements using stainless steel plates, while filled triangles are measurements with the ERO apparatus. Data points a, b, and c correspond to conoscopic images in Figure 3.

those obtained with the stainless steel plates. Comparison of the steady-state electroviscosity at a shear rate of 0.1 s^{-1} obtained with both sets of plates is shown in Figure 2. In all subsequent figures, the electric field reported for the ERO apparatus is the corrected one.

Experimental Results

Electrorheooptical Experiment. Conoscopic interference patterns in the ERO apparatus of a 30% PHIC solution taken at various electric field strengths and a shear rate of 0.1 s^{-1} are displayed in Figure 3. The interference pattern consists of a series of concentric circles and a cross located at the center of the circles. The crosslike figure and its center are called an isogyre and a melatope, respectively. For uniaxial crystals, the position of the melatope reflects the orientation of the optical axis.[26] Figure 3d shows the interference pattern of a homeotropically aligned quiescent PHIC solution in which the melatope is located at the center, indicating that the optical axis of the PHIC solution is perpendicular to the picture. For a uniaxial nematic liquid crystal, the optical axis of the material and the director coincide,[28] so that by comparing the interference patterns in a shear flow with that of a homeotropic orientation, the melatope displacement indicates the tilting of the director from the electric field axis. Our ERO setup only allowed us to observe the innermost circle and the isogyre clearly; we estimate that only tilt angles within about 15° from the electric field axis can be seen in this apparatus. In Figure 3, the flow direction is from top to bottom as indicated by the arrow, and the electric field is perpendicular to the pictures as indicated by the "X". Below 0.3 MV/m, no interference image was visible at 0.1 s^{-1}. With increasing electric field strength (Figure 3a,b), the melatope (emphasized by the white cross) moved opposite the flow direction (i.e., the director aligned more closely with the field direction); the same occurred when a fixed electric field was applied and the shear rate was lowered. At a shear rate of 0.1 s^{-1} and electric field strength of 1.4 MV/m, the interference pattern under shear flow (Figure 3c) was virtually indistinguishable from that of the homeotropic orientation (Figure 3d), demonstrating that the viscosity measured under these conditions is the Miesowicz viscosity η_c.

The ERO experiments validate important assumptions and results of the two-dimensional Doi theory. The appearance of the interference patterns demonstrates the uniaxial and unidomain structure of the LCP solutions. Since the interference patterns are symmetric with respect to the shear flow, the rotation of the director is confined to the plane of the velocity gradient (defined to be the plane containing the velocity gradient and the flow direction), thus supporting the two-dimensional approximation. Furthermore, at low shear rates and applied fields, the conoscopic interference pattern was obliterated, suggesting director tumbling of PHIC solutions under these conditions.

Steady-State Electroviscosity and Normal Stress. In this section the effects of shear rate, electric field, concentration, and temperature on the steady-state normal stress and electroviscosity are presented. In Figure 4, the shear stress of a 30 wt % PHIC solution is plotted as a function of shear rate for various electric fields. The zero-field shear stress increases monotonically with shear rate. At the lowest electric field of 0.4 MV/m, the shear stress exhibits a broad maximum between shear rates of 0.3 and 1 s^{-1}. Some suspension ER fluids also exhibit a maximum and/or minimum in their stress−shear rate curves.[29−32] Above 10 s^{-1}, the shear stress curve at 0.4 MV/m collapses onto the curve for zero electric field, suggesting that shear rate effects dominate electric field effects above 10 s^{-1}. Thus, we consider a shear rate of 10 s^{-1} a convenient demarcation between low and high shear rate regimes. At higher electric fields, the shear stress increases, and the observed maximum shifts to higher shear rates. The highest shear stress observed for this PHIC solution is 16 kPa at 4 MV/m and 30 s^{-1}, which is comparable to the observed stress of a strong suspension ER fluid. At the lowest shear rate of 0.1 s^{-1}, the transmitted stress at 4 MV/m is 180 times that without electric field, while at the highest shear rate of 100 s^{-1} and 4 MV/m, the steady-state electroviscosity is 26 times the zero-field steady-state stress. Low shear rate zero-field and plateau electroviscosities are tabulated for each studied concentration in Table 1. The plateau viscosities were estimated by extrapolating high field data to $1/E^2 \rightarrow 0$; correlation coefficients R always exceeded 0.984.

The steady-state electroviscosity as a function of electric field for shear rates ranging from 0.3 to 50 s^{-1} of a 28 wt % PHIC solutions is shown in Figure 5. For shear rates less than 10 s^{-1}, the steady-state electroviscosity increases with increasing electric field in a sigmoidal fashion and approaches a plateau viscosity at low shear rates. The viscosity enhancement, defined to be the ratio of the plateau viscosity to the zero-field steady-state viscosity, is 116 ± 24. For shear rates of 10 s^{-1} or larger, a threshold electric field exists below which the electric field has a negligible effect on the viscosity. This threshold electric field appears to increase with shear rate. At a shear rate of 30 s^{-1}, the threshold field is about 0.8 MV/m. Above the threshold electric field, the electroviscosity starts to increase with electric field, but the electric field strengths used were not high enough for the electroviscosity to approach a plateau value. At a fixed electric field, the viscosity exhibits shear thinning behavior.

The corresponding normal stress of a 28 wt % solution is plotted in Figure 6, with values for a quiescent sample included for comparison. The normal stress measured at shear rates of 0.3 s^{-1} and that measured under quiescent conditions are virtually indistinguishable and are always negative, indicating that the plates are pulled together. The quiescent normal stress arises from the attraction exerted by the oppositely charged plates

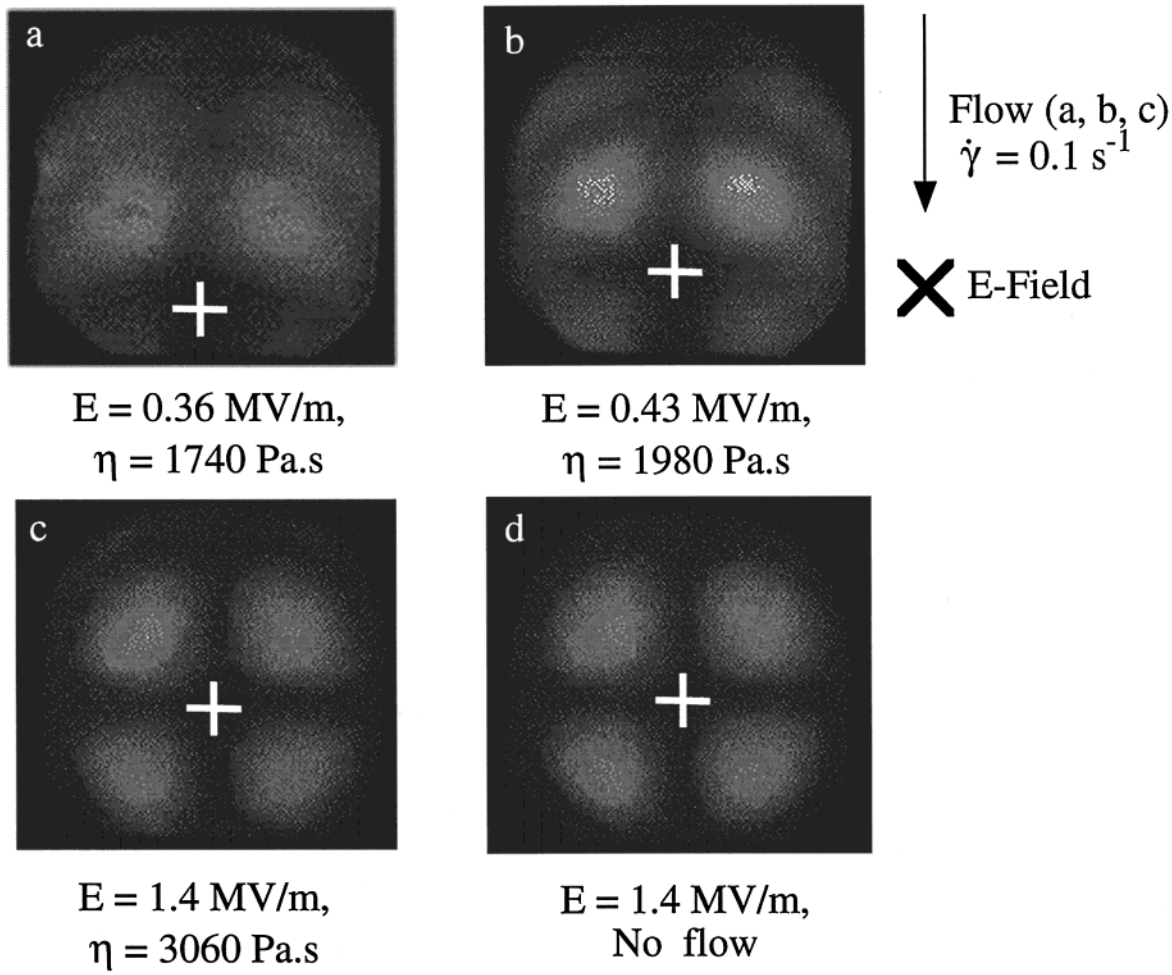

Figure 3. Conoscopic interference patterns for a 30 wt % PHIC solution. Flow direction is from top to bottom, and electric field direction is into the page. (a), (b), and (c) were taken at a shear rate of 0.1 s^{-1}, while (d) is a quiescent sample. Corresponding electric fields and measured viscosities are indicated below each pattern.

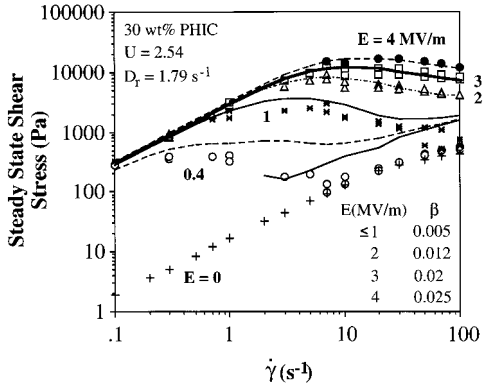

Figure 4. Shear stress of a 30 wt % PHIC solution as a function of shear rate for various dc electric field strengths. Symbols and lines are data and model predictions, respectively. β as a function of electric field strength is also reported. (+, E = 0 MV/m; ○, E = 0.4 MV/m; *, E = 1 MV/m; △, E = 2 MV/m; □, E = 3 MV/m; ●, E = 4 MV/m).

on each other. The behavior of the normal stress in the high shear rate regime is more complicated. For a 28 wt % solution, it is small and positive at small electric fields, indicating the parallel plates are pushed apart by the LCP solution. With increasing electric field, the normal stress increases, reaches a maximum, and finally starts to decrease and becomes large and negative. The electric field at which the maximum of the normal stress occurs is slightly above the threshold electric field in the electroviscosity plot of Figure 5, suggesting that the ER effect is also reflected in the normal stress measurements.

The effect of concentration at room temperature was also studied so as to determine whether concentration is an important parameter in fluid formulation. Results of the electroviscosity of 26, 28, and 30 wt % PHIC solutions as a function of shear rate at electric fields of 0.4 and 2 MV/m are shown in Figure 7. At an electric field of 2 MV/m, the steady-state electroviscosity at low shear rates increased from 1730 Pa·s for a 26 wt % solution to 3130 Pa·s for 30 wt %, while the viscosity enhancement increased from 99 for the 26 wt % solution to 180 times for 30 wt %. However, the effect of concentration is mitigated when the effect of shear rate begins to dominate, since the plateau viscosity is not achieved at high shear rates and reasonable electric fields.

One of the harshest demands on practical ER fluids is the requirement to function over a wide range of temperatures. The normal stress and the steady-state electroviscosity of PHIC solutions were also measured at 13, 37, and 52 °C. (The freezing point of *p*-xylene is 12 °C.) The steady-state electroviscosity of a 30% PHIC solution at a shear rate of 0.3 s^{-1} is shown in Figure 8 for four different temperatures. At 2 MV/m, the electroviscosity decreased from 3400 Pa·s at 13 °C to 2200 Pa·s at 52 °C, a drop of about 30% over nearly 40 °C.

Table 1. Summary of Model Parameters and Results of Steady-State Measurements of PHIC Solutions at Room Temperature

conc, wt %	no. conc c ($\times 10^{-24}$ molecules/m^3)	U	D_r (s^{-1}) ± std dev	zero-field viscosity (Pa·s) ± std dev	plateau electroviscosity (Pa·s) ± std error
26	1.40	2.33	2.69 ± 0.11	17.4 ± 1.0	1730 ± 100
28	1.52	2.43	2.20 ± 0.14	19.2 ± 2.6	2230 ± 160
30	1.63	2.54	1.79 ± 0.09	17.2 ± 1.2	3130 ± 190

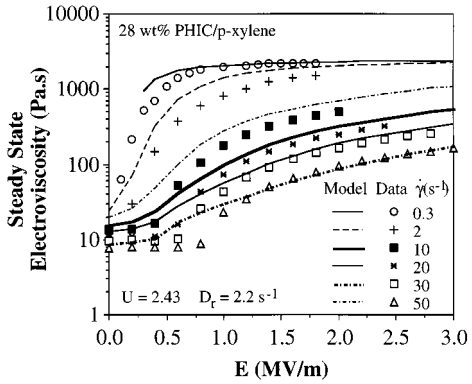

Figure 5. Electroviscosity of a 28 wt % PHIC solution as a function of dc electric field strength at room temperature. Symbols and lines are data and model predictions, respectively. The calculations were performed with the parameters tabulated in Table 1. Values of β tabulated in Figure 4 and scaled for concentration were used for shear rates larger than 10 s^{-1}.

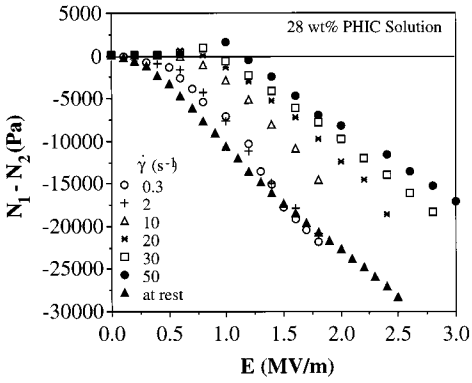

Figure 6. Normal stress of a 28 wt % PHIC solution as a function of electric field strength for various shear rates at room temperature.

The activation energy of the electroviscosity at 2 MV/m and a shear rate of 0.3 s^{-1} was determined to be 7 ± 1.3 MJ/kg·mol, which is similar to that of the steady-state zero-field viscosity in the low shear rate limit (9.6 ± 2 MJ/kg·mol) as well as that of *p*-xylene (8.8 MJ/kg·mol).[33] These results suggest that the polymer molecules can be treated as nearly athermal even in the presence of an electric field and that the temperature sensitivity of an ER LCP solution can be minimized by choosing a solvent with an activation energy as small as possible.

Since the electrorheooptical study showed that the plateau electroviscosity corresponds to the Miesowicz viscosity, η_c, our temperature study suggests that η_c of PHIC solutions decreases with increasing temperature. This is consistent with the temperature dependence observed in low molecular weight liquid crystals, such as *p′*-methoxybenzylidene-*p*-*n*-butylaniline and *p*-*n*-hexyloxybenzylidene-*p′*-aminobenzonitrile,[34] but in contrast to suspension ER fluids where increased charge mobility at increased temperatures can lead to large increases in transmitted stress.

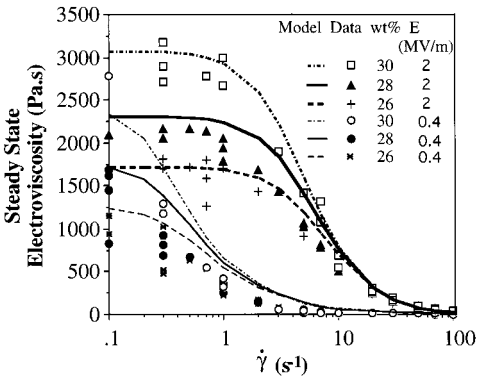

Figure 7. Concentration dependence of steady-state electroviscosity of PHIC solutions at dc electric fields of 0.4 and 2 MV/m and room temperature. Symbols and lines are data and model predictions, respectively. The predictions were calculated with the parameters tabulated in Table 1.

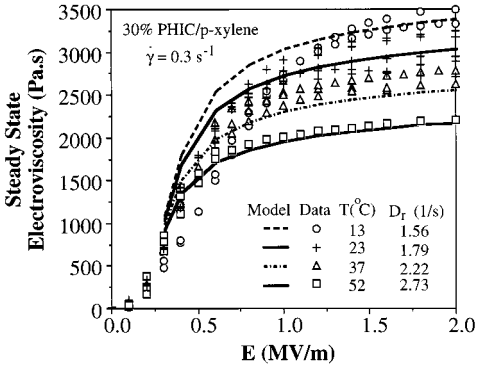

Figure 8. Effect of temperature on steady-state electroviscosity of a 30 wt % PHIC solution at a shear rate of 0.3 s^{-1}. Symbols and lines are data and model predictions.

Modeling

The experimental characterization of the ER properties of the PHIC solutions presented in the previous section has established a rich database for testing the two-dimensional model based on Doi theory developed earlier[18] and reviewed briefly below. Here, we model the concentration, temperature, shear rate, and electric field dependence of the steady-state viscosity. Unfortunately, the normal stress difference, $N_1 - N_2$, in the presence of shear and electric fields cannot be modeled because the two-dimensional approximation does not allow the normal stress difference to vanish in parallel plate geometry in the absence of shear and electric fields.[26]

A uniform electric field is applied across parallel plates bounding a unidirectional shear field, as shown schematically in Figure 9. Following the developments of Marrucci and Maffettone,[19] the Smoluchowski diffusion equation governing the molecular orientation distribution function, $f(\phi,t)$, is

$$\frac{\partial f}{\partial \tau} = \frac{\partial}{\partial \phi}\left(\frac{\partial f}{\partial \phi} + f\frac{\partial (V/kT)}{\partial \phi}\right) + \frac{\partial}{\partial \phi}(\dot{\alpha} f + G\cos^2(\alpha + \phi)) \quad (1)$$

where τ is a dimensionless time, $\tau = tD_r$, t is time, D_r is

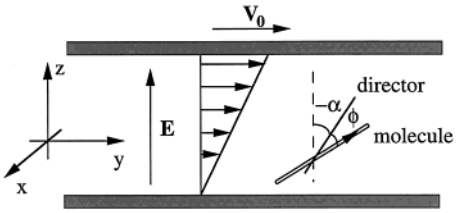

Figure 9. Geometry of two-dimensional modeling. The upper plate moves with constant velocity V_0.

the rotational diffusivity which is assumed to be constant, α is angle the director makes with the electic field direction, $\dot{\alpha}$ is the dimensionless time derivative of α, ϕ is the angle between a molecule and the director, and $G = \dot{\gamma}/D_r$ is the dimensionless shear rate. The potential V is given by the sum of of the Maier−Saupe nematic potential and the potential of a permanent dipole in an electric field:

$$\frac{V(\phi)}{kT} = -US(\cos 2\phi) - (\mu g E/kT)\cos(\alpha + \phi) \quad (2)$$

where U is the strength of the nematic potential, S is the order parameter, μ is the molecular dipole moment, g is the Onsager cavity field factor which is assumed to be 1.5, E is the strength of the applied electric field, and kT is the product of the Boltzmann constant and absolute temperature. The general solution to eq 1 was obtained by expanding the orientation distribution function as a Fourier series, and employing the principle of virtual work, to solve numerically for the elastic contribution to the stress tensor, $\boldsymbol{\sigma}^{\mathbf{E}}$. The relevant component of the shear stress is given by

$$\frac{\sigma_{21}^{E}}{ckT} = -\sin 2\alpha\langle\cos 2\phi\rangle - \frac{1}{2}U\langle\cos 2\phi\rangle(\sin 2\alpha(\langle\cos 4\phi\rangle - 1) + \cos 2\alpha\langle\sin 4\phi\rangle) - \frac{1}{4}E'(\sin\alpha\langle\cos\phi\rangle + \cos\alpha\langle\sin\phi\rangle + \sin 3\alpha\langle\cos 3\phi\rangle + \cos 3\alpha\langle\sin 3\phi\rangle) \quad (3)$$

where the angled brackets denote averaging over configuration space. The values of these averaged quantities are given by the Fourier coefficients of the orientation distribution function.

At small shear rates, this elastic component dominates the total stress.[19] According to this 2-D model, the electrorheology is governed by the three dimensionless groups: U (the strength of the nematic potential), $E' = g\mu E/kT$ (a dimensionless electric field), and $G = \dot{\gamma}/D_r$ (the dimensionless shear rate). Since g, μ, E, and T are known quantities, and U is determined from the solution concentration, D_r is the only parameter needed to determine $\boldsymbol{\sigma}^{\mathbf{E}}$ and thus the electroviscosity at low shear rates. D_r was determined at each experimental concentration by least-squares fitting of the electroviscosity data at a shear rate of 0.3 s^{-1} and electic fields ≥0.9 MV/m. Table 1 lists the values of D_r thus determined, as well as the U values for each concentration. The strength of the nematic potential, U, was estimated from Doi theory for a given c/c^*, where c is the number concentration and c^* is the critical concentration; c values are also tabulated in Table 1. In the calculations, we have used the viscosity-average molecular weight in

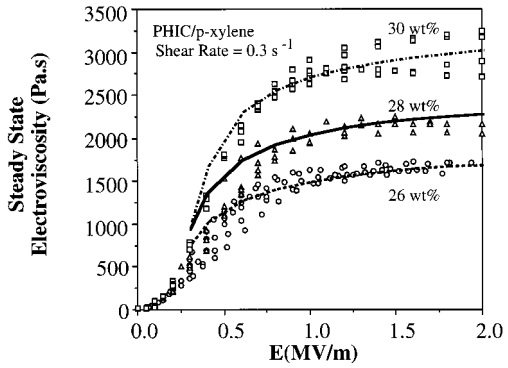

Figure 10. Effect of concentration on electroviscosity at room temperature and 3 s^{-1}. Symbols and lines are data and model predictions, respectively.

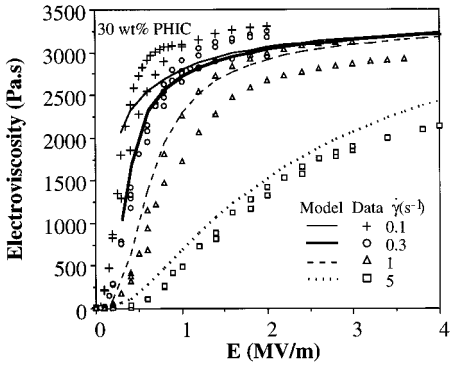

Figure 11. Electroviscosity of 30 wt % PHIC solutions at low shear rates. Symbols and lines are data and model predictions, respectively.

the estimation of c and the dipole moment, although the model presumes a monodisperse polymer. The three fitted values of D_r show a concentration dependence to the power −2.66 ± 0.42, as compared with predictions from Doi theory of −2.0.

Figure 10 shows the best fit of the model to room-temperature electroviscosity data at each concentration and a shear rate of 0.3 s^{-1}. In the electric field range where D_r was fitted (0.9−2 MV/m), the deviation of data from model was comparable to the standard error of measurement. However, the model predictions are systematically higher than measured values for lower fields. Below an applied field of 0.3 MV/m, the model predicts the absence of a steady-state solution due to director tumbling. Just above this critical field value, the director of the 30 wt % solution was predicted to be aligned at a 45° angle from the field direction.

Using the D_r values fit to the 0.3 s^{-1} data, it is possible to predict the electroviscosity at other shear rates; predictions for the 30 wt % solution for low shear rates are shown in Figure 11. Above 10 s^{-1}, the electroviscosity was systematically underpredicted by as much as 50%, with agreement worst at high fields and high shear rates. We believe that this discrepancy arises from neglecting the viscous contribution to the stress tensor under these conditions.

Unlike the elastic stress, which arises from energy storage in the system, the viscous stress arises from the friction between the polymer molecules and the solvent and is responsible for viscous heat dissipation in the system. The elastic and viscous stresses of LCP solutions have been measured by the stress jump technique developed by Smyth and Mackay.[35]

For the geometry of Figure 9, the viscous contribution to the stress tensor, $\boldsymbol{\sigma}^{\mathbf{v}}$, as derived by Marrucci and Maffettone is

$$\frac{\boldsymbol{\sigma}^{\mathbf{v}}}{ckT} = \beta G(1 - \cos 4\alpha\langle\cos 4\phi\rangle + \sin 4\alpha\langle\sin 4\phi\rangle) \quad (4)$$

The parameter β is defined by Doi and Edwards[36] to be

$$\beta = \frac{D_r}{8D_{r0}} \quad (5)$$

where D_{r0} is the rotational diffusivity in the dilute solution limit, and β is known to be much smaller than unity.[19] D_{r0} can be estimated for rodlike polymers from molecular parameters[37] as

$$D_{r0} = \frac{3kT(\ln(L/b) - 0.8)}{\pi\eta_s L^3} \quad (6)$$

where L is the rod length, b is the rod diameter, and η_s is the solvent viscosity. In principle, we can directly estimate β from eqs 5 and 6 using estimates of the molecular dimensions of PHIC. However, following Marrucci and Maffettone,[19] we treat β as an empirically adjustable parameter in the high shear rate regime.

The data of the 30 wt % PHIC solution in Figure 4 were used to determine the best values of β, which are shown in Figure 4 for electric fields of 1, 2, 3, and 4 MV/m. For electric fields $\leq$1 MV/m, β was taken as 0.005, while above 1 MV/m, it appeared to increase nearly linearly with electric field. For shear rates $\leq$10 s^{-1}, the viscous stress was ignored in the calculations.

The model is seen to capture the essential features of the steady-state electroviscous stress. Although for a given concentration D_r was determined at a shear rate of 0.3 s^{-1}, and is treated only as a function of concentration, the model is able to describe the shear rate and electric field dependence of the data. Agreement between predicted and measured shear stress improves as electric field is increased. The model reproduces the maximum in the stress curve and is capable of describing the shift of the maximum to higher shear rates with increasing electric field. As pointed out by Marrucci and Maffettone,[19] this maximum is a characteristic of the elastic stress. At a shear rate of 100 s^{-1}, the model predicted that the elastic stress contributed 44−48% of the total shear stress for electric fields ranging from 1 to 4 MV/m. Calculations were also carried out for the case of zero field. The model overpredicts the zero-field shear stress or viscosity by about a factor of 2. Director tumbling caused no steady-state solutions to exist at zero field for shear rates less than 2 s^{-1}.

Since the rotational diffusivities at concentrations of 26, 28, and 30 wt % have been determined from the steady-state electroviscosity data at 0.3 s^{-1}, the model can be used to describe the steady-state electroviscosity or shear stress at high shear rates if the concentration dependence of β is known. According to eq 5, β and D_r have the same concentration dependence. Since β of a 30 wt % solution as a function of electric field has been estimated, β at the other concentrations was obtained by scaling it with the rotational diffusivity at the desired concentration, i.e., $\beta(c) = \beta(30\text{ wt }\%)D_r(c)/D_r(30\text{ wt }\%)$. Figure 5 shows model predictions for the electroviscosity of a 28 wt % PHIC solution, while predictions for all experimental concentrations at electric field strengths of 0.4 and 2 MV/m are shown as the lines in Figure 7. Both figures show better agreement between calculated and measured values at higher fields.

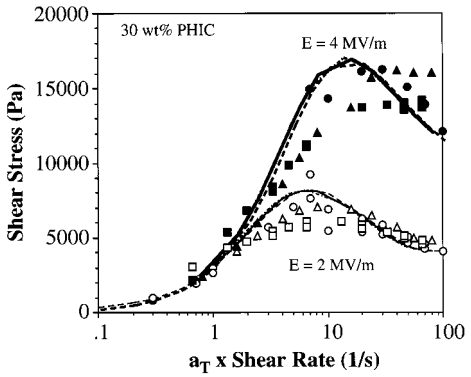

Figure 12. Time−temperature superposition: shear stress of a 30 wt % PHIC solution at various temperatures. Filled symbols and thick lines are data and model predictions, respectively, at $E = 4$ MV/m. Open symbols and thin lines are data and model predictions, respectively, at $E = 2$ MV/m. Squares and solid lines, 52 °C; triangles and dashed lines, 37 °C; circles and dotted lines, 23 °C.

Experimental measurements of the zero-field and elecroviscosities suggest that the temperature dependence is strongly influenced by the temperature dependence of the solvent. The ability to predict LCP solution ER behavior based solely on knowledge of the solvent behavior would be a distinct advantage to ER device designers, especially in comparison with suspension ER fluids. The temperature dependence of the model parameters D_r and β must be known in order to make a priori predictions of the temperature behavior of the ER properties.

The temperature dependence of D_r arises directly from D_{r0}. Since D_{r0} scales with T/η_s, D_r at other temperatures can be obtained if the viscosity of *p*-xylene as a function of temperature is known. The viscosity of *p*-xylene from temperatures of 270 to 410 K has been published elsewhere[33] and was used to scale D_r for different temperatures on the basis of the experimentally determined D_r value at room temperature. The estimated rotational diffusivity of a 30 wt % PHIC solution at the other three temperatures is also reported in Figure 8 and increases from 1.56 s^{-1} at 13 °C to 2.73 s^{-1} at 52 °C. For a given electric field, the predicted electroviscosity at a shear rate of 0.3 s^{-1} decreases with increasing temperature. In the plateau region, quantitative agreement between the predictions and data is seen at these four temperatures.

Predicting the effect of temperature on the shear stress or electroviscosity in the high shear rate regime requires knowledge of the temperature dependence of β. Since a shear rate independent β provided an excellent description of the shear stress, it is reasonable to assume β to be a function of only electric field, and the same values shown in Figure 4 were used for the 30 wt % solution at other temperatures. Predictions as well as experimental data of a 30 wt % PHIC solution at electric fields of 2 and 4 MV/m and at shear rates ranging from 1 to 100 s^{-1} are plotted in Figure 12. Here, we have employed the principle of time−temperature superposition to correlate the steady-state data collected at different temperatures by plotting them as a function of the reduced shear rate defined as $a_T\dot{\gamma}$. Because of the weak temperature dependence of the nematic and

dipolar potential terms in the model, the shift factor a_T was estimated as $D_r(23\ °C)/D_r(T)$, where $D_r(T)$ is the rotational diffusivity at the experimental temperature and 23 °C was chosen as the reference state. Both the experimental data and the model predictions form master curves, proving the applicability of time−temperature superposition to unidomain LCPs in the presence of electric fields. These results suggest that the temperature dependence of the steady-state electroviscosity or shear stress of an LCP solution is primarily due to the solvent. Of course, this is true only over temperature ranges which have no thermodynamic phase transitions.

Conclusions

In this work, we have experimentally studied the steady-state ER properties of 100 000 $\overline{M}_v$ PHIC/*p*-xylene solutions over 3 decades of shear rate, a 39 °C temperature range, concentrations from 26 to 30 wt %, and electric field strengths from 0 to 4 MV/m. The ER behavior was successfully modeled using a two-dimensional version of Doi's molecular theory of LCP rheology. Electrorheooptical measurements confirmed the unidomain and two-dimensional assumptions of the model and that the plateau viscosity observed at high electric fields corresponds to the transverse Miesowicz viscosity, η_c. At low shear rates, the temperature, shear rate, and electric field dependence of the viscosity could be described using a single concentration-dependent parameter, the rotational diffusivity D_r. At shear rates above 10 s^{-1}, it was necessary to adopt an additional parameter, β, to account for viscous contributions to the stress tensor. β was empirically found to be a nearly linear function of electric field strength but independent of shear rate. The concentration dependence of β mimics that of D_r, so high shear rate data could also be predicted by the model over the experimental range of shear rate, electric field strength, concentration, and temperature.

Fundamentally very different from suspension ER fluids, these LCP solutions nevertheless exhibited many desirable ER properties, such as high transmitted stress (16 kPa) and large viscosity ratio (180*X*). Their main disadvantages appear to be a high zero-field viscosity and reduced influence of electric field at high shear rates.

The predictability of the Doi model for describing ER properties of LCPs is far superior to models available for describing suspension ER fluids. Most significantly, because Doi theory is a molecular theory, it is possible at low shear rates to develop a priori predictions of the ER behavior as a function of shear rate, temperature, and concentration, directly from the rod dimensions, dipole moment, and solvent viscosity. This insight should aid designers in formulating LCP solutions to optimize the ER properties for specific applications and in developing control schemes to be used with ER devices.

Acknowledgment. It is a pleasure to acknowledge financial support from the National Science Foundation under Grant CMS-9402397.

References and Notes

(1) Winslow, W. M. *J. Appl. Phys.* **1949**, *20*, 1137.
(2) Parthasarathy, M.; Klingenberg, D. J. *Mater. Sci.* **1996**, *R17*, 57−103.
(3) Rankin, P. J.; Ginder, J. M.; Klingenberg, D. J. *Curr. Opin. Coll. In.* **1998**, *3*, 373−381.
(4) Stanway, R.; Sproston, J. L.; El-Wahed, A. K. *Smart Mater. Struct.* **1996**, *5*, 464−482.
(5) Inoue, A.; Maniwa, S. *J. Appl. Polym. Sci.* **1995**, *55*, 113−118.
(6) Kimura, H.; Minagawa, K.; Koyama, K. *Polym. J.* **1994**, *26*, 1402−1404.
(7) Yao, N.; Jamieson, A. M. *Macromolecules* **1997**, *30*, 5822−5831.
(8) Chiang, Y. C.; Jamieson, A. M.; Kawasumi, M.; Percec, V. *Macromolecules* **1997**, *30*, 1992−1996.
(9) Lee, Y. C.; Huh, J. D.; Chung, I. J *Polym. J.* **1990**, *22*, 295−303.
(10) Yang, I. K.; Shine, A. D. *J. Rheol.* **1992**, *36*, 1079−1104.
(11) Tse, K. L.; Shine, A. D. *Polym. Prepr.* **1994**, *35* (2), 383−384.
(12) Yang, I. K.; Huang, I. T. *J. Polym. Sci., Polym. Phys.* **1997**, *35*, 1217−1224.
(13) Tanaka, K.; Takahashi, A.; Akiyama, R. *Phys. Rev. E* **1998**, *58*, R1234−R1236.
(14) Tanaka, K.; Takahashi, A.; Akiyama, R.; Kuramoto, N. *Phys. Rev. E* **1999**, *59*, 5693−5696.
(15) Carlsson, T.; Skarp, K. *Mol. Cryst. Liq. Cryst.* **1981**, *78*, 157−171.
(16) Brochard, F. *J. Polym. Sci., Polym. Phys. Ed.* **1979**, *17*, 1367−1374.
(17) Doi, M. *J. Polym. Sci.* **1981**, *19*, 229−243.
(18) Tse, K.-L.; Shine, A. D. *J. Rheol.* **1995**, *39*, 1021−1039.
(19) Marrucci, G.; Maffettone, P. L. *Macromolecules* **1989**, *22*, 4076−4082.
(20) Marrucci, G.; Maffettone, P. L. *J. Rheol.* **1990**, *34*, 1217−1230.
(21) Shashoua, V. E.; Sweeny, W. E.; Tiets, R. F. *J. Am. Chem. Soc.* **1960**, *82*, 866.
(22) Itou, T.; Chikiri, H.; Teramoto, A.; Aharoni, S. M. *Polym. J.* **1988**, *20*, 143−151.
(23) Onsager, L. *Ann. N. Y. Acad. Sci.* **1949**, *51*, 627.
(24) Block, H.; Gosling, J. J.; Walker, S. M. *Polymer* **1984**, *25*, 1465−1468.
(25) Blinov, L. M.; Chigrinov, V. G. *Electrooptical Effects in Liquid Crystal Materials*; Springer-Verlag: New York, 1994.
(26) Wahlstrom, E. E. *Optical Crystallography*, 5th ed.; John Wiley and Sons: New York, 1979.
(27) Tse, K. L. Ph.D. Dissertation, University of Delaware, 1996.
(28) DeGennes, P. G. *The Physics of Liquid Crystals*; Clarendon Press: Oxford, 1974.
(29) Block, H.; Kelly, J. P. *J. Phys. D: Appl. Phys.* **1988**, *21*, 1661−1677.
(30) Sprecher, A. F.; Carlson, J. D.; Conrad, H. *Mater. Sci. Eng.* **1987**, *95*, 187−197.
(31) Xu, Y.-Z.; Liang, R.-F. *J. Rheol.* **1991**, *35*, 1355−1373.
(32) Korobko, E. V.; Shulman, Z. P. In *Electrorheological Fluids*; Carlson, J. D., Sprecher, A. F., Conrad, H., Eds.; Technomic: PA, 1990.
(33) Viswanath, D. S.; Natarajan, G. *Data Book on the Viscosity of Liquids*; Hemisphere: New York, 1989.
(34) Gähwiller, C. *Mol. Cryst. Liq. Cryst.* **1973**, *20*, 301.
(35) Smyth, S. R.; Mackay, M. E. *J. Rheol.* **1994**, *38*, 1549−1558.
(36) Doi, M.; Edwards, S. F. *J. Chem. Soc., Faraday Trans. 2* **1978**, *74*, 918−932.
(37) Doi, M.; Edwards, S. F. *The Theory of Polymer Dynamics*, Clarendon Press: Oxford, 1986.

MA991585O